Improvements in the Beam-Mismatch Correction of Precipitation Radar Data After the TRMM Orbit Boost

Kaya Kanemaru, Takuji Kubota, *Member, IEEE*, and Toshio Iguchi, *Fellow, IEEE*

***Abstract*— The orbit of the tropical rainfall measuring mission (TRMM) satellite was boosted from 350 to 402.5 km in August 2001 to extend its lifetime by conserving fuel. Since the timing between transmission and reception by the precipitation radar (PR) onboard the TRMM satellite was a fixed constant for measurement from an original altitude of 350 km, the PR encountered a mismatch between the transmitting and receiving beams after the TRMM orbit boost. Although the PR algorithm in TRMM Version 7 employs a correction for the beam mismatch, its error remains as an underestimation of the precipitation estimates near surface in the second half of the swath. This paper aims to mitigate the beam-mismatch correction error in Version 7. The beam-mismatch correction needs to estimate the radar echo that would be measured in the virtual intermediate beam between the beam in question and the previous adjacent beam. The beam-mismatch correction developed in this paper assumes that the surface and precipitation echoes change linearly in the horizontal direction in parallel to the surface between the two beams. The new correction is tested with observational data, indicating that the method improves the accuracy of the correction at off-nadir angles. Statistics of the surface normalized radar cross sections and the bright band peak intensities at off-nadir angles are improved using the method. The asymmetric bias of the precipitation estimates with respect to the scan angle in Version 7 is mitigated by 95.9% over ocean and 72.5% over land with the new correction.**

***Index Terms*— Algorithm, beam mismatch, precipitation radar (PR), tropical rainfall measuring mission (TRMM).**

I. Introduction

THE precipitation radar (PR) onboard the Tropical Rainfall Measuring Mission (TRMM) [1], [2] satellite is the first spaceborne radar observing the vertical structure of precipitation. The observation by the PR continued for more than 17 years from December 1997 to April 2015, much longer than originally expected, thanks to the TRMM orbit boost in August 2001. The TRMM satellite flew at a low altitude compared to other orbiting remote sensing satellites so that its orbit was easily lowered by a drag due to the earth atmosphere and a large amount of fuel was required to maintain its altitude. In August 2001, the TRMM orbit was boosted from 350 to 402.5 km to reduce the drag and save the fuel.

The PR data quality has changed slightly due to the TRMM orbit boost. The impact of the TRMM orbit boost on precipitation estimates by the PR can be divided into three categories: sensitivity degradation, degradation of horizontal resolution, and the effects of the beam mismatch [3], [4]. The sensitivity degradation is degradation of the minimum detectable precipitation echo. Since received power from precipitation decreases with an increase in the distance despite unchanged noise power, degradation of signal-to-noise ratio results in missing light precipitation. The degradation of horizontal resolution elevates the height of clutter-free bottom in off-nadir beams. The PR's beamwidth is 0.71° so that the horizontal resolution changes from 4.3 to 5 km due to the TRMM orbit boost. Since scattering volume around the surface at off-nadir angles includes surface echo, its contamination reaches at a higher elevation and covers the echoes from shallow precipitation. On the other hand, the beam mismatch is specific to the PR's issue.

The details of the beam mismatch were described by Takahashi and Iguchi [3]. The beam mismatch is caused by a fixed pulse repetition frequency of the PR and by the constant catching integer that defines the delay of switching the receiving beam direction to the transmitting beam direction in terms of the number of pulse repetition intervals. It transmits a pulse at a constant frequency of 2776 Hz. The echoes by the first pulse from precipitation near surface are received between the seventh and eighth transmitting pulses. Therefore, the receiving beam direction is not changed simultaneously with the transmitting direction, but delayed by seven pulses. After the orbit change, the echoes from near surface fell between the eighth and ninth transmitting pulses. The receiving window of pulses is fixed so that the last transmitted pulse at one scan angle is returned as the first received pulse at the next scan angle. As a result, the PR observation from 402.5 km was contaminated by the mismatch between transmission and reception beams [3]. The contamination of the beam mismatch after the TRMM orbit boost was corrected to some extent in the PR's level-1 algorithm. The method reported by Takahashi and Iguchi [3] (hereafter TI04) was implemented in the PR's Version 7 (V7) product. The accuracy of the TI04 method was found to be 0.2 dB for precipitation echo and 0.5 dB for surface echo [3]. However, a residual error of the beam-mismatch correction in V7 affected the precipitation estimates. Shimizu *et al.* [4] showed that the precipitation

Manuscript received October 29, 2018; revised January 9, 2019 and March 26, 2019; accepted April 15, 2019. Date of publication May 15, 2019; date of current version August 27, 2019. This work was supported by the National Institute of Information and Communications Technology. *(Corresponding author: Kaya Kanemaru.)*

K. Kanemaru and T. Iguchi are with the National Institute of Information and Communications Technology, Koganei 184-8795, Japan (e-mail: kanemaru@nict.go.jp).

T. Kubota is with the Earth Observation Research Center, Japan Aerospace Exploration Agency, Tsukuba 305-8505, Japan.

Color versions of one or more of the figures in this article are available online at http://ieeexplore.ieee.org.

Digital Object Identifier 10.1109/TGRS.2019.2911990

0196-2892 © 2019 IEEE. Translations and content mining are permitted for academic research only. Personal use is also permitted, but republication/ redistribution requires IEEE permission. See http://www.ieee.org/publications_standards/publications/rights/index.html for more information.

estimates sorted by the PR's cross-track scan angle (angle-bin number) had a bias caused by the imperfect beam-mismatch correction that results in an underestimation of precipitation rate by an average of 2.9% over all angle-bin numbers. Tagawa *et al.* [5] propose an improved correction method (hereafter T09) to mitigate the error around the surface echoes and the angle-bin dependence of precipitation estimates. However, the correction error around a bright band remains in the T09 method.

An improvement in the beam-mismatch correction is important not only to estimate precipitation rates accurately but also to produce a stable long-term precipitation record. In February 2014, the Core Observatory of the Global Precipitation Measurement (GPM) mission [6], [7] was launched and the observation with the dual-frequency PR (DPR) began. The DPR comprises the Ku-band PR (KuPR), whose frequency of 13.6 GHz is nearly the same as the TRMM PR's 13.8 GHz, and the Ka-band PR (KaPR) with a frequency of 35.5 GHz. The sensor design of the DPR is almost identical to the PR; however, the delay time of the DPR between the transmitting pulse and the receiving window is variable so that the DPR does not have a beam mismatch issue as the PR. Observations with PR and DPR overlapped for ∼1 year so that we can create a continuous and consistent 20-year record of precipitation observations by Ku-band spaceborne radars of PR and KuPR. Since the residual error of the beam-mismatch correction affects ∼3% of the precipitation estimates, a systematic difference between PR and KuPR causes an inhomogeneity in the long-term precipitation record obtained using spaceborne radars.

Further improvement of the beam-mismatch correction is required to utilize the long-term observation obtained using PR and DPR for climate analysis. This paper aims to improve the beam-mismatch correction. A method developed herein is implemented in the PR level-1 data processing in TRMM Version 8 (V8) released in October 2017. We review the past beam-mismatch correction methods and describe the improvement proposed in this paper in Section II. In Section III, the new method of beam-mismatch correction is evaluated. The findings are summarized in Section IV.

II. Method of Beam-Mismatch Correction

A mechanism of the beam-mismatch and its correction method are briefly reviewed. Details of the beam-mismatch correction are described by previous studies [3], [5].

The PR samples 32 pulses to improve the accuracy of measurement and downlinks data that are logarithmically averaged. Note that the PR employs two-frequency agility so that the actual sampling number is 64 [8]. The received power $P_{r,\mathrm{obs}}$ measured by the PR is expressed as follows:

$$P_{r,\mathrm{obs}}(n,m) = \frac{1}{32}\sum_{i=1}^{32} P_{r,i}(n,m) \tag{1}$$

where n and m are the angle-bin number ($n = 1,\ldots,49$) and range-bin number, respectively. The angle-bin number represents a cross-track scan angle, which is expressed as $(25-n)\times 0.71^\circ$ in the PR observation, and the range-bin number indicates a range distance relative to the distance at the first sampling range bin at $n = 25$. The received power P_r is expressed in decibel space (dBm), which is $P_r = 10\log_{10}(p_r)$, and p_r is expressed in real space (mW). Hereafter, the upper (lower) case is in decibel (real) space. After the TRMM orbit boost, one of the 32 pulses is included as a mismatched pulse and averaged together. Therefore, the observation of the received power after the TRMM orbit boost $P_{r,\mathrm{BMobs}}$ is expressed as follows:

$$P_{r,\mathrm{BMobs}}(n,m) = \frac{1}{32}\left[\sum_{i=1}^{31} P_{r,i}(n,m) + P_{r,\mathrm{mb}}\right] \tag{2}$$

where $P_{r,\mathrm{mb}}$ is the received power of the mismatched beam. Since the beam-mismatch correction involves removing the contamination of the mismatched power, a corrected received power $P_{r,\mathrm{BMcor}}$, which is equivalent to an average of 31 pulses, is obtained as follows:

$$\begin{aligned} P_{r,\mathrm{BMcor}}(n,m) &= \frac{1}{31}\sum_{i=1}^{31} P_{r,i}(n,m) \\ &= \frac{1}{31}\left[32P_{r,\mathrm{BMobs}}(n,m) - P_{r,\mathrm{mb}}\right]. \end{aligned} \tag{3}$$

As shown in (3), the accuracy of the beam-mismatch correction depends on the estimation accuracy of $P_{r,\mathrm{mb}}$. Since the two-way antenna pattern of the mismatched Gaussian beams peaks in the center of the angle between the $(n-1)$th transmitting beam and the nth receiving beam, the radar echoes received by the combination of the mismatched beams are equivalent to the echoes received by the virtual intermediate beam between the current nth and adjacent $(n-1)$th beams. Hereafter, we call the intermediate beam as the $(n-1/2)$th beam. Methods estimating the echoes measured by the mismatched beams are described in Sections II-A–II-C.

A. TI04 (V7) Method

The PR observation from 402.5 km was not originally envisioned so that the beam-mismatch correction by TI04 was developed in a limited time. The correction by the TI04 method was adopted as a standard algorithm in the TRMM V7 product. The estimate of the mismatched power by TI04 is expressed as follows:

$$P_{r,\mathrm{mb(TI04)}} = \max\left\{10\log_{10}(p_r') - 6,\, P_n(n)\right\} \tag{4}$$

where P_n is the noise power. p_r' is given as follows:

$$p_r' = \frac{1}{2}[p_{r,\mathrm{BMobs}}(n,m) + p_{r,\mathrm{BMobs}}(n-1,m)]. \tag{5}$$

The offset of −6 dB originates from the gain change caused by the mismatch of the $(n-1)$th transmitting and nth receiving beam directions.

The beam-mismatch correction by TI04 works well at near-nadir angles, but the correction causes some errors at off-nadir angles. Fig. 1 schematizes the geometry between the radar and the earth's surface. At near-nadir angles shown in Fig. 1(a), the beam enters vertically against the earth's surface and precipitation. If we assume that precipitation and surface echoes are horizontally uniform, similar echoes are expected

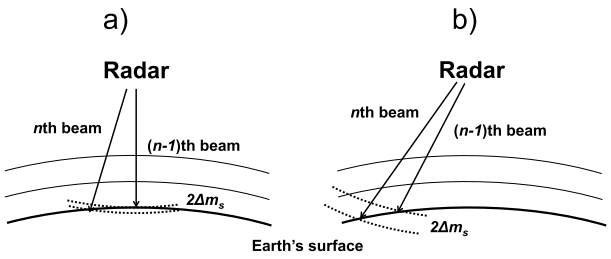

Fig. 1. Schematic of the spaceborne radar geometry. Arrows show the vector of the radar scan along the cross-track direction. Solid lines: same height against the earth's surface. Dashed lines: same range from the radar. (a) Near-nadir case. (b) Off-nadir case.

at the same range-bin number in two adjacent beams. Since echo profiles among $(n-1)$th, $(n-1/2)$th, and nth beams are similar, the $(n-1/2)$th beam is correctly estimated by using (5) at near nadir angles. However, at off-nadir angles [Fig. 1(b)], the beam does not enter vertically against the earth's surface so that the heights from the earth's surface are different for the range bins with the same bin number in two adjacent beams. The difference in the height from the surface in this case can be simply estimated. We assume a flat surface and use satellite height H and scan angle θ. The range from the satellite to the surface r_s is represented as $H/\cos\theta$. We also use the range from the satellite r and height from the surface z. Then, z is expressed as follows:

$$z = (r_s - r)\cos\theta = H - r\cos\theta. \tag{6}$$

The height $z + \Delta z$ at the same range r for $\theta + \Delta\theta$ is

$$z + \Delta z = H - r\cos(\theta + \Delta\theta). \tag{7}$$

Therefore, Δz is obtained as follows:

$$\begin{aligned}\Delta z &= H - r\cos(\theta + \Delta\theta) - (H - r\cos\theta) \\ &= r\cos\theta - r\cos(\theta + \Delta\theta) \\ &\simeq \Delta\theta r\sin\theta.\end{aligned} \tag{8}$$

In the case of $\Delta\theta = 0.71°$ and $r = 402.5$ km, Δz is smaller than 0.2 km when the scan angle is less than $\sim 2°$, but Δz increases with scan angle and exceeds 1 km when the scan angle is $> 12°$. Thus, the accuracy of $(n-1/2)$th beam echoes at off-nadir angles by TI04 depends not only on the horizontal patterns of surface and precipitation echoes but also on the vertical profiles. The horizontal resolution of the PR at 402.5 km is ~5 km so that the ground clutter reaches 2–3 km at off-nadir angles [5]. Since the surface echo drastically changes nonlinearly with the height around the surface, a vertical change in the surface echo between nth and $(n-1)$th beams results in the error at off-nadir angles if the linear interpolation expressed in (5) is used. This kind of error also occurs around a bright band where the vertical gradient of the precipitation echo is steep. TI04 reported that these errors at off-nadir angles reach 0.2 dB for the bright band echo and 0.5 dB for the near-surface echo. The error of the received power near the surface results in a negative bias of radar reflectivity factor Z, which causes the underestimation of precipitation R by 2.9% averaged over all angle-bin numbers [4]. In the PR algorithm, the Z–R relation for the stratiform type is initially adopted to $Z = 298.84\ R^{1.38}$ [9]. Therefore, the beam-mismatch correction error in decibel space ΔZ_{dB} is inferred from a relative bias of ΔR, that is,

$$\Delta Z_{\mathrm{dB}} = 1.38 \times 10\log_{10}(1 + \Delta R). \tag{9}$$

The underestimation of precipitation estimates in the V7 product corresponds to $1.38\times10\log_{10}(1-0.029) = -0.18$-dB bias of Z or P_r, which is comparable to the residual error of the TI04 method reported.

B. T09 Method

The T09 method improves the beam-mismatch correction by TI04 to mitigate the error around surface echoes. In the T09 method, the surface echo of the mismatched beam is directly estimated, then the mismatched power is given as follows:

$$P_{r,\mathrm{mb(T09)}} = 10\log_{10}\left(p_r''\right) \tag{10}$$

and

$$\begin{aligned}p_r'' = {} & w_1(n,m)[p_{r,\mathrm{BMobs}}(n-1,m) - p_n(n-1)] \\ & + w_2(n,m)[p_{r,\mathrm{BMobs}}(n,m) - p_n(n)\ ] + p_n(n)\end{aligned} \tag{11}$$

where w_1 and w_2 are the weighting functions. w_1 and w_2 are determined by a numerical result of the mismatched echo pattern and changes with n and m around the surface echoes. T09 showed the improvement in the estimates for surface echoes. An importance of the T09 method is to geometrically calculate the mismatched echo pattern. The TI04 correction assumes a linear change of echo between the adjacent beams. The assumption is generally valid near nadir but it does not necessarily hold at off-nadir angles. The T09 correction estimates surface echoes of the mismatched beam by a geometric calculation of the echoes with the mismatched antenna pattern; thus, the T09 method mitigates the error around surface echoes at off-nadir angles. The weighting factors w_1 and w_2 for precipitation echoes from the mismatched beam by T09 are assumed to be $w_1(n,m) = w_2(n,m) = 1/8 = -9$ dB so that (11) becomes

$$p_r'' = \frac{1}{8}\left[2p_r' - p_n(n-1) - p_n(n)\right] + p_n(n). \tag{12}$$

Equation (12) is essentially the same as the TI04 method except for noise power. Since the TI04 method has some error around the bright band peak, the T09 method also maintains the error around bright band echoes.

C. Method Developed in This Paper

The methods of the beam-mismatch correction reported previously can be summarized as follows. The TI04 method assumes that the echoes can be linearly interpolated at the same range in two consecutive beams. The assumption is not necessarily valid at off-nadir angles and causes a bias of the received power around the surface and a bright band. The T09 method improves the estimates for the surface echoes from the mismatched beams by geometrically calculating the

mismatched echo pattern, but the error around a bright band remains.

Based on the previous studies, the method of beam-mismatch correction in this paper assumes that echo profiles of adjacent beams are similar and change linearly in horizontal directions at each height from the surface. From this assumption, the estimate of received power from the mismatched beams is obtained as follows:

$$P_{r,\mathrm{mb(New)}} = \max\left\{10\log_{10}\left(p_r'''\right) - 6,\, P_n(n)\right\} \tag{13}$$

and

$$p_r''' = \frac{1}{2}[p_{r,\mathrm{BMobs}}(n, m+\Delta m_s) + p_{r,\mathrm{BMobs}}(n-1, m-\Delta m_s)] \tag{14}$$

where Δm_s is $[m_s(n) - m_s(n-1)]/2$ and m_s is the range-bin number of the earth's surface. Equation (14) is similar to the TI04 method except for the shifting of the range-bin number. The beam-mismatched correction developed in this paper simply assumes that the echoes from mismatched beams can be obtained by linear interpolation between the nth and $(n-1)$th beams in parallel to the earth's surface, which roughly estimates the echoes from the mismatched beam directions at off-nadir angles. Although this correction is somewhat less accurate than the T09 correction, the method has an advantage of simplicity and is applicable to the correction of both precipitation and surface echoes at off-nadir angles. Since (14) needs m_s at the nth and $(n-1)$th beams, this paper utilizes "binDIDHmean" in the level-1 standard product. "binDIDHmean" is the range-bin number at surface elevation by computing the geolocation and digital elevation model. If the absolute difference in m_s is less than 2, i.e., $|\Delta m_s| < 2$, then Δm_s is assumed to be 0. When observations at $m + \Delta m_s$ or $m - \Delta m_s$ are not contained in the product, data are obtained by the linear interpolation of adjacent range-bin data in decibel space. Except for these details, the correction method in this paper follows the TI04 method.

III. Results

A. Impact on Level-1 Products

The method of the beam-mismatch correction developed in this paper is confirmed by the PR external calibration data taken before the TRMM orbit boost. In the calibration mode, the PR scan pattern is spatially oversampled two times in the cross-track direction [8]; then, the scan angle of $(n_{\mathrm{ext}}/2-1)$th beam where n_{ext} is the angle-bin number for the external calibration mode ($n_{\mathrm{ext}} = 1, \ldots, 103$) is equivalent to that of the operational nth beam and is expressed as $n_{\mathrm{ext}} = 2\,n + 2$. Therefore, the nth and $(n-1/2)$th beams for the operational mode can be obtained as the $(2\,n+2)$th and $(2\,n+1)$th beams in the external calibration mode. Here, simulated data of the received power from the mismatched beams $P_{r,\mathrm{BMsim}}$ are calculated as follows:

$$P_{r,\mathrm{BMsim}}(n, m) = \frac{1}{32}[31P_{r,\mathrm{obs}}(n, m) + \max\{P_{r,\mathrm{obs}}(n-1/2, m) - 6,\, P_n(n)\}]$$

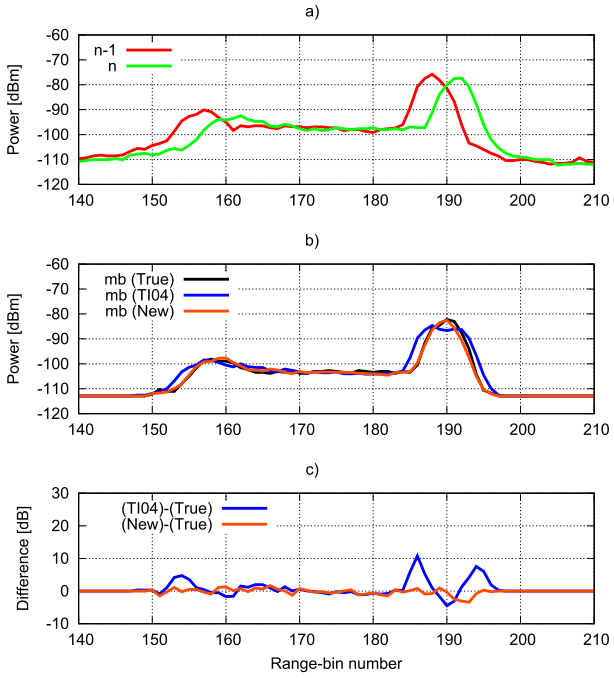

Fig. 2. Snapshot of received power profiles obtained by the PR external calibration mode (2001/07/17 orbit 20930 at scan angle of $-7.1°$ that is $n = 35$ or $n_{\mathrm{ext}} = 72$). The horizontal axis is the range-bin number. In this case, a precipitation profile with bright band is observed over land. (a) Simulated beam-mismatched power (dBm) at the nth and $(n-1)$th beams calculated in (15). (b) Estimated mismatched power (dBm) at the $(n-1/2)$th beam. Black line: true power at the $(n-1/2)$th beam measured at $n_{\mathrm{ext}} = 71$. Blue and orange lines: the estimated profile of the mismatched power by the TI04 method and that by the new method from the simulated beam-mismatched power shown in Fig. 2(a), respectively. (c) Differences in power (dB) between the true power and TI04 (new) estimates in blue (orange) color.

$$= \frac{1}{32}[31P_{r,\mathrm{ext}}(2n+2, m) + \max\{P_{r,\mathrm{ext}}(2n+1, m) - 6,\, P_{n,\mathrm{ext}}(2n+2)\}] \tag{15}$$

where $P_{r,\mathrm{ext}}$ and $P_{n,\mathrm{ext}}$ are the received power and noise power obtained in the external calibration mode, respectively. Once the beam-mismatch echo is simulated by (15) with the external calibration data, simulated data are used to validate the mismatched echoes estimated in the beam-mismatch correction. The mismatched beams by the TI04 method in (4) and those by the new method in (14) are estimated with the simulated data and compared with the $(n-1/2)$th beam echoes that correspond to the true echoes from the mismatched beams. Fig. 2 shows the case of precipitation with a bright band over land. The angle-bin number of this case corresponds to $n = 35$ in the observation mode. As shown in Fig. 2(a), the received power profiles at angle-bin numbers n and $n-1$ are similar except for the difference in the range-bin number. Surface peaks in the $(n-1)$th and nth beams are located at 188 and 192, respectively, so that the difference in surface peaks is ~4 range bins or 500 m (1 range bin is ~125 m). Since the TI04 method estimates the mismatched power by averaging two beams at the same range bins, it estimates the surface echo at $(n-1/2)$th beam [blue line in Fig. 2(b)] much wider than the true power of the mismatched beam [black line in Fig. 2(b)]. Similar errors are also found around the bright band located at

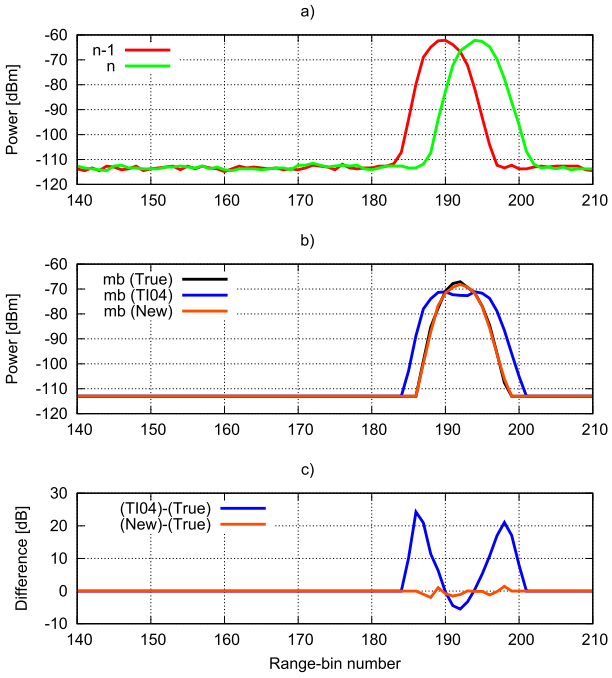

Fig. 3. Same as Fig. 2, but over ocean in a nonprecipitating case.

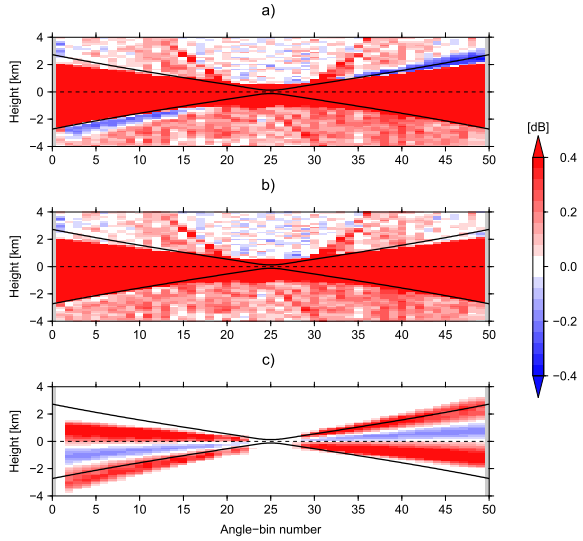

Fig. 4. Vertical cross section of the difference in power (dB) between the received power and noise power. The horizontal axis is the angle-bin number and the vertical axis is the height from the earth's surface. Solid lines: boundaries of cluttered ranges calculated in [11]. Data over ocean are averaged with scan numbers from 601 to 700 of orbit number 21 650 at 2001/09/01. (a) V7. (b) New. (c) Difference between V7 and new products. Note that data are interpolated along the range-bin number when oversampled data does not exist.

range-bin numbers from 152 to 162, whereas the new method [orange line in Fig. 2(b)] accurately estimates the surface and bright band echoes by the mismatched beam. The new method assumes that the surface peak of the mismatched beam is at the range-bin number of 190 and that its profile is obtained from the average between the nth and $(n-1)$th beams after both profiles are parallelly shifted in such a way that their peaks match at range bin 190. Differences in power between true and estimates are shown in Fig. 2(c). The new method shows a small error relative to the true power, whereas the TI04 method has a large error of surface echo at range bins from 185 to 196 and the bright band echo at the range bin 154. Since the beam mismatch is corrected by subtracting the mismatched power profiles divided by 31 from the observation as shown in (3), an overestimation of the mismatched power by 10 dB results in an overcorrection or a negative bias in the total power by $\sim$0.3 dB. Fig. 3 indicates another example in a nonprecipitating case over ocean with the same external calibration data at the same scan angle. The result in this case is similar to Fig. 2, but the error of the mismatched power by the TI04 method is greater than the error over land. The overestimation is maximally 20 dB at range bins 186 and 198 [Fig. 3(c)]. Since the normalized radar cross section or σ^0 over ocean is greater than over land at off-nadir angles [10], the overestimation of the mismatched power around the surface over ocean becomes greater than over land. The mismatched power profile estimated by the new method is quite similar to the true power [Fig. 3(b)] and its difference is small [Fig. 3(c)] compared with the TI04 method.

To evaluate impacts on level-1 products, the new beam-mismatch correction is implemented into the PR power (1B21) product and compared to the original V7 product. Fig. 4 shows the vertical cross section of the received power anomaly from noise power over ocean. The boundaries of cluttered ranges calculated in [11] are also drawn. Since the PR's fading noise is $\sim$0.70 dB and higher than the beam-mismatch correction error in the V7 products, the 100-scan data in a nonprecipitating scene are averaged to reduce the fading noise. The result of the V7 product [Fig. 4(a)] shows that a negative bias is found at the lower bound of the main lobe in the first half (FH) scans (angle bins from 2 to 15) and at the upper bound in the second half (SH) scans (angle bins from 35 to 49). In the case of no precipitation, the received power should be the same as the noise power except at the ranges cluttered by the surface echo because no precipitation echo exists above the clutter-free-bottom height. However, the V7 product shows unnatural negative power anomalies around the clutter-free-bottom height [Fig. 4(a)] in nonprecipitating cases. This negative bias in the V7 product arises from the inaccurate estimates of the mismatched surface echo. The same bias is expected to remain in a precipitating scene. The bias of power around the clutter-free-bottom height reaches -0.3 dB in the SH scans, which propagates the bias of -5% for precipitation estimates given in (9). The negative bias of power in the V7 product is located below the surface in the FH scans and above the surface in the SH scans so that the negative bias for precipitation estimates appears in only the SH scans. By contrast, the negative bias found in the V7 product around the clutter-free-bottom height is hardly observed in the new beam-mismatch correction [Fig. 4(b)]. The unbiased power anomalies around the clutter-free areas shown in Fig. 4(b) indicate that the new beam-mismatch correction reasonably estimates the power profiles at the clutter-free areas compared with the original beam-mismatch correction. A difference between V7 and new products [Fig. 4(c)] is observed when the

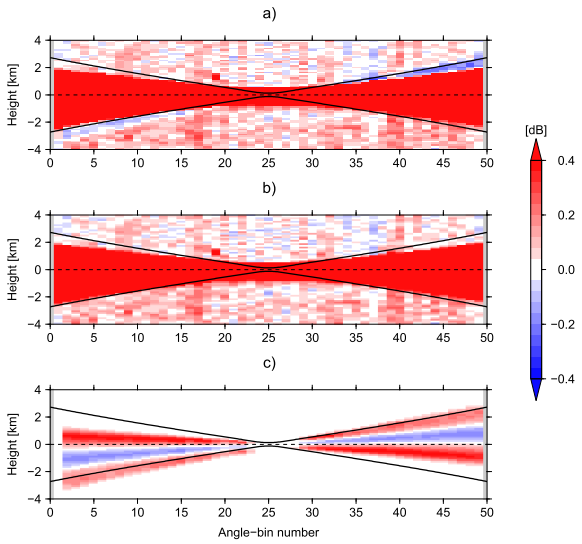

Fig. 5. Same as Fig. 4, but over land where scan numbers are from 8001 to 8100.

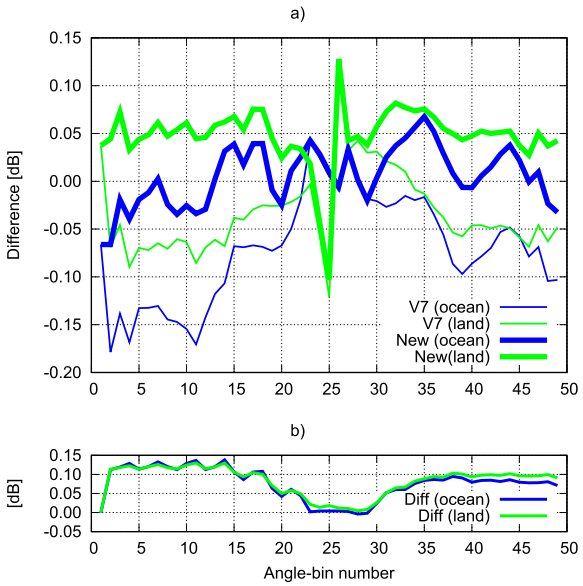

Fig. 6. Angle-bin dependence of the difference in σ^0 (dB) between preboost and postboost periods. σ^0 in nonprecipitating pixels are averaged within the latitudinal band between 35°S and 35°N. The postboost period is 1-year average from September 2001 to August 2002. The preboost period is the same but from August 2000 to July 2001. (a) V7 over ocean (blue solid) and over land (green solid). The new product is drawn as bold lines over ocean (blue) and land (green). (b) Difference between V7 and new products over ocean (blue) and land (green).

new correction mitigates the overcorrection of the V7 product around the main lobe edges, which is similar to the T09 result. The original beam-mismatch correction estimates surface echoes of the mismatched beam too wide so that it reaches the clutter-free region and results in the negative bias of power there. The new beam-mismatch correction improves the mismatched power of surface echoes, which mitigates the negative bias around the top of the main lobe surface clutter. Fig. 5 shows another case over land. The difference between V7 and new products over land is similar to the case over ocean in Fig. 4. A negative bias is found to be ~0.2 dB around the main lobe edge in the SH scans [Fig. 5(a)], whereas this bias is not clearly visible in the new method [Fig. 5(b)]. The difference between V7 and new products [Fig. 5(c)] is similar to the case over ocean.

B. Impact on Level-2 Products

In this section, impacts of the new beam-mismatch correction to level-2 products are examined by comparing with the V7 product. The level-2 rainfall (2A25) product is generated from the 1B21 product via the products of level-1 radar reflectivity (1C21), level-2 radar cross section (2A21), and rain characteristics (2A23) products. The level-2 products are reprocessed using the 1B21 product with the new beam-mismatch correction for 1 year from September 2001 to August 2002. None of the algorithms are modified at all, except for the 1B21 algorithm.

Fig. 6(a) shows the angle-bin dependence of the difference in σ^0 between preboost and postboost periods. The difference in σ^0 obtained by the V7 product over ocean (blue solid) and land (green solid) has a jump between $n = 1$ and $n = 2$. The accuracy of the beam-mismatch correction at $n = 1$ is greater than the other angle bins because the mismatched power can be simply assumed as the noise power for the first angle bin. Moreover, the σ^0 difference at off-nadir angles ranges up to 0.15 dB over ocean and 0.10 dB over land. The difference arises mainly from the error of the beam-mismatch correction for the surface echo. In contrast to the V7 product, the σ^0 difference obtained from the product developed in this paper shows no abrupt jump between $n = 1$ and $n = 2$. The angle-bin dependence of the σ^0 difference is mitigated over both ocean (blue bold) and land (green bold), which indicates that the continuity of σ^0 between preboost and postboost periods is improved by the new beam-mismatch correction. The steep angle-bin dependence of the σ^0 difference at nadir angles over land is caused by a small change in the incident angle between preboost and postboost periods. Since σ^0 over land has a steep negative slope with an increase in the incident angle [3], the small change in the incident angle causes the σ^0 difference. In the current analysis, the incident angles of $n = 24$ and $n = 25$ have increased by $\sim 0.03°$, whereas the incident angle of $n = 26$ has decreased by $\sim 0.01°$ since the change of the orbit attitude. As a result, σ^0 at $n = 25$ has decreased, but σ^0 at $n = 26$ has increased over land. The difference between V7 and new products is shown in Fig. 6(b). At near-nadir angles, the new method of beam-mismatch correction is quite similar to the V7 method so that σ^0 remains almost unchanged. At off-nadir angles, except for the first angle bin, the new product increases σ^0 by 0.1 dB over ocean and land.

Fig. 7 shows the impact on the statistics of the measured Z or Z_m at the bright band peak. Z_m at the bright band peak is obtained by the 2A23 product [12] and averaged conditionally as a function of the angle-bin number. Although the difference in Z_m at the bright band peak between preboost and postboost periods has an angle-bin dependence [Fig. 7(a)], the difference between V7 and new products [Fig. 7(b)] is

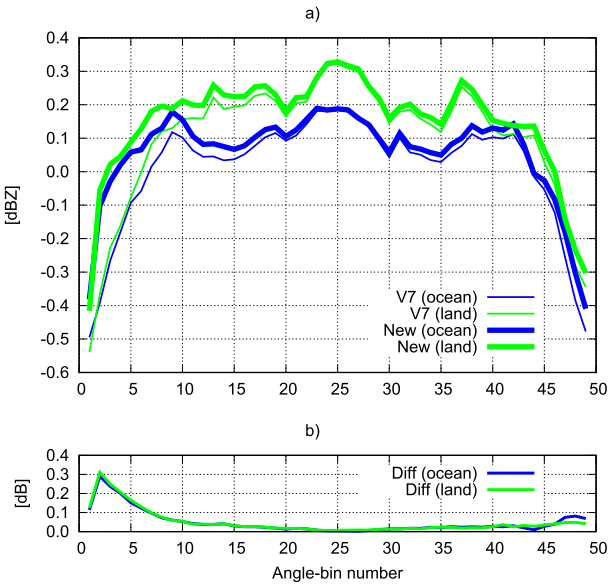

Fig. 7. Same as Fig. 6, but the difference in Z_m (dB) at the bright band peak.

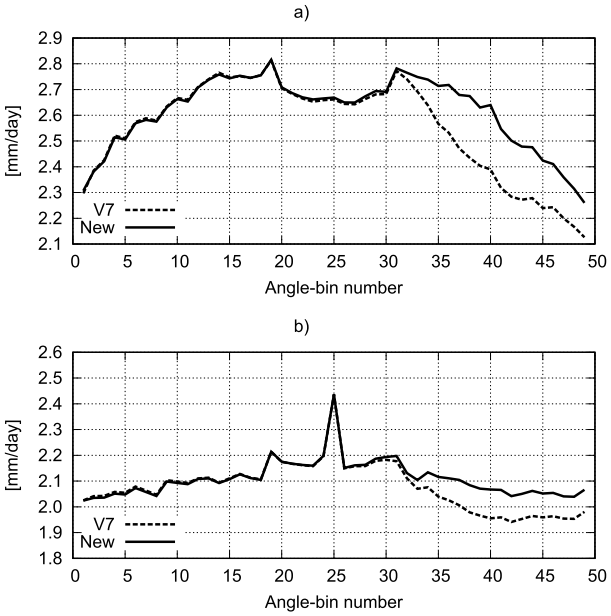

Fig. 8. Angle-bin dependence of precipitation estimates (mm day^{-1}) obtained from September 2001 to August 2002 within the latitudinal band between 35°S and 35°N. Dashed and solid lines: V7 and new products, respectively. (a) Over ocean. (b) Over land.

clearly found in the FH angles and maximally increased by ~0.3 dB. The beam-mismatch correction at $n = 1$ is the same as the TI04 method, but Z_m at the bright band peak at $n = 1$ increases slightly by the new method. Since the detection of the bright band adopts spatial filtering [12], an improvement in the bright band detection at $n = 2$ may affect the bright band detection at $n = 1$ and change the Z_m statistics at the bright band.

An improvement in the beam-mismatch correction for precipitation estimates is evaluated by comparing the data produced by the new method with the original 2A25 product [13]. Fig. 8 shows the 1-year average of near-surface rain sorted by

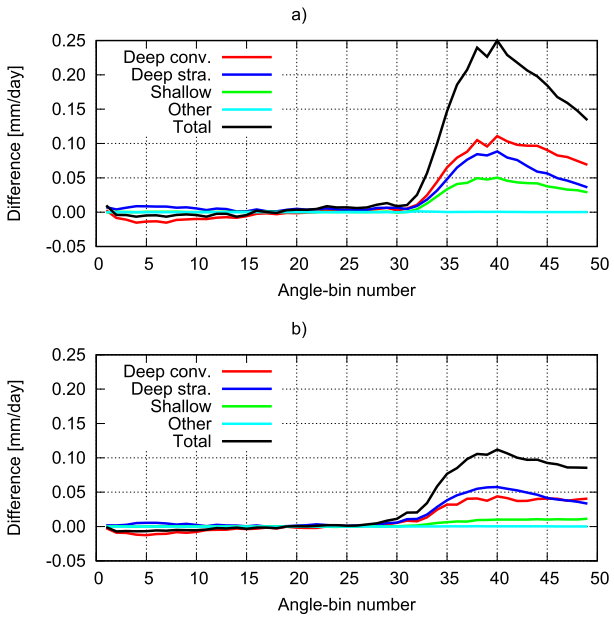

Fig. 9. Angle-bin dependence of the difference in precipitation amount (mm day^{-1}) between V7 and new products. The difference in the total precipitation (black) is divided into deep convective (red), deep stratiform (blue), shallow (green), and other (cyan) types. (a) Over ocean. (b) Over land.

the angle bin. Since the angle-bin dependence of precipitation estimates and the changes of the beam-mismatch correction are different between over ocean and land, the differences in precipitation estimates between V7 and new products over ocean and land are separately evaluated. The V7 products underestimate the precipitation amount in the SH scans compared with that in the FH scans over ocean [Fig. 8(a)] and land [Fig. 8(b)]. These underestimations are propagated from the negative anomaly of power at the main lobe edge in SH scans of the level-1 product as shown in Figs. 4(a) and 5(a). The negative anomaly of power above the surface is seen only in the SH scans so that the beam-mismatch correction error for precipitation estimates is found as negative bias only in the SH scans. By contrast, the precipitation estimates obtained using the new product increase in the SH scans compared with V7 so that obvious underestimations are mitigated. Since the negative bias of power at the main lobe edge in SH scans is hardly seen in the level-1 product [Figs. 4(b) and 5(b)], the improvement of beam-mismatch correction increases power and resultant precipitation in SH scans.

Fig. 9 indicates the difference in precipitation estimates between V7 and new products by precipitation types. The precipitation type is categorized using a shallow rain flag ("flagShallowRain") and rain type flag ("rainType") in the 2A23 product. Here, a deep convective (stratiform) type is categorized as nonshallow rain of the convective (stratiform) type. Shallow type is categorized as shallow rain of both convective and stratiform types. Another type is adopted as it is by the other of rainType. Over ocean [Fig. 9(a)], an increase in the total precipitation amount in the SH scans has a peak at $n = 40$. A slight decrease in total precipitation in the FH scans comes from a small decrease in deep convective type

TABLE I

ASYMMETRIC BIAS OF PR'S PRECIPITATION ESTIMATES (%) OVER OCEAN AND LAND. FH AND SH ARE AVERAGED BY ANGLE-BIN NUMBERS FROM 1 TO 25 AND FROM 25 TO 49, RESPECTIVELY. THE PREBOOST (POSTBOOST) DATA ARE ANALYZED FROM 1998 TO 2000 (FROM 2002 TO 2008) WITHIN THE LATITUDINAL BAND BETWEEN 35° AND 35°N

(SH -FH)/FH	Ocean [%]	Land [%]
V7 pre-boost	−0.36	+0.07
V7 post-boost	−5.26	−4.01
Post − Pre	−4.90	−4.08

TABLE II

SAME AS TABLE I, BUT 1-YEAR AVERAGE FROM SEPTEMBER 2001 TO AUGUST 2002 OBTAINED BY V7 AND NEW PRODUCTS

(SH -FH)/FH	Ocean [%]	Land [%]
V7	−6.31	−3.25
New	−1.61	−0.29
New − V7	+4.70	+2.96

that overcomes a small increase in deep stratiform type. This decrease may be caused by the change in precipitation type due to the detection of the bright band in Fig. 7. Over land [Fig. 9(b)], the increase in the total precipitation amount in the SH scans is explained by the increases in the deep convective and deep stratiform types. The decrease in the FH scans over land is similar to the change over ocean.

The improvement in the beam-mismatch correction is quantitatively assessed in terms of an asymmetric bias of precipitation estimates. Here, the asymmetric bias of precipitation estimates ΔR_{asym} is defined as follows:

$$\Delta R_{\text{asym}} = \frac{R_{\text{SH}} - R_{\text{FH}}}{R_{\text{FH}}} \tag{16}$$

where R_{FH} and R_{SH} are the averages of precipitation estimates in angle bins from 1 to 25 (FH) and from 25 to 49 (SH), respectively. Table I outlines the ΔR_{asym} obtained by V7 during the preboost period of 3 years from 1998 to 2000 and the postboost period of 7 years from 2002 to 2008. ΔR_{asym} during the preboost period is obtained as -0.36% over ocean and 0.07% over land, but ΔR_{asym} during the postboost period is -5.26% over ocean and -4.01% over land. Since the beam-mismatch correction error for precipitation estimates occurs only during the postboost period, the difference in ΔR_{asym} between preboost and postboost periods is found as the bias in the beam-mismatch correction error for precipitation estimates. Thus, the beam-mismatch correction error in V7 is obtained as the difference in ΔR_{asym} of -4.90% $(= -5.26 + 0.36)$ over ocean and -4.08% $(= -4.01 - 0.07)$ over land. The same assessment during 1 year of the postboost period is performed for V7 and new products (Table II) to evaluate impacts of the new beam-mismatch correction on precipitation estimates. ΔR_{asym} of the V7 product is calculated as -6.31% over ocean and -3.25% over land, whereas ΔR_{asym} of the new product is -1.61% over ocean and -0.29% over land. Therefore, the new beam-mismatch correction changes ΔR_{asym} by $+4.70\%$ $(= -1.61 + 6.31)$ over ocean and $+2.96\%$ $(= -0.29 + 3.25)$ over land from the V7 product. Assuming that the beam-mismatch correction error of ΔR_{asym} is obtained by the difference between preboost and postboost periods and is mitigated by the new product against the V7 product, the correction error of the new method for ΔR_{asym} is -0.20% $(= 4.70 - 4.90)$ over ocean and -1.12% $(= 2.96 - 4.08)$ over land. Thus, new method improves ΔR_{asym} by ratios of 95.9% $(= 1 - 0.20/4.90)$ over ocean and 72.5% $(= 1 - 1.12/4.08)$ over land. The improvement over land slightly degrades in comparison with that over ocean due to the difficulty in estimating the surface echoes of the mismatched beam by the current and adjacent beams in complex topography. Moreover, since the new method shifts the range of adjacent beam based on the range difference in the surface echo peaks (Δm_s), if the adjacent surface height changes significantly, the interpolation for beam-mismatch correction is not horizontal but parallel to the surface slope. As a result, over a steep terrain, even if the bright band echo is horizontal at a constant height above the sea level, the beam-mismatch correction with the current method may not work well for the bright band. The errors caused by this kind of limitations are beyond this paper and left for future improvements.

IV. CONCLUSION

In this paper, we describe a method that improves the beam-mismatch correction for the PR data after the TRMM orbit boost by mitigating some remaining error in the V7 product. We first verified the performance of the new method with simulated beam-mismatched data created from the PR data taken in the external calibration mode. To verify the improvement in the beam-mismatch correction and to evaluate its impact on precipitation estimates in real data, intercomparisons between the standard V7 product and data processed with the new method are conducted.

The beam-mismatch correction requires the echo profile that would be measured by the mismatched beam corresponding to the intermediate beam between the beam in question and the previous adjacent beam. Thus, how to correctly estimate such an echo profile from the available data is the key to the correction method. The method reported by Takahashi and Iguchi [3] and implemented in the V7 product assumes that radar reflectivity changes linearly in space in two consecutive beams. Since this assumption is not appropriate for surface echo or bright band echo, the mismatched power at off-nadir angles is erroneously estimated. The error of the beam-mismatch correction for the surface echo results in the underestimation of precipitation estimates at the SH of the cross-track scan. In the method developed herein, the mismatched power is estimated by a spatial interpolation between two adjacent beam profiles at the same height from the earth's surface with the assumption that the spatial pattern of the surface and precipitation echoes are linearly distributed in parallel to the earth's surface between two adjacent beams. With this simple assumption, the correction errors for surface and bright band echoes in the V7 product are mostly mitigated. The statistics of the incident angle dependence of σ^0 obtained by the new correction method becomes continuous and shows no abrupt changes between before and after the TRMM orbit

boost. Since the beam-mismatch correction in this paper works well at the bright band, the statistics of Z_m at the bright band peak at off-nadir angles is improved from the V7 product. The improvement in the precipitation estimates is evaluated in terms of the asymmetric bias in the cross-track scan. The asymmetric bias between the first and SH scans is obviously observed in the V7 product, whereas that of the new product is fairly mitigated. The mitigation of asymmetric biases by the new beam-mismatch correction method is estimated to be 95.9% over ocean and 72.5% over land. The improvement over land slightly degrades than that over ocean, which is a limitation of the new method in complex topography.

The PR level-1 data in the TRMM V8 product are reprocessed with the beam-mismatch correction developed in this paper and released in October 2017. The reprocessed PR data will provide precipitation estimates consistent with KuPR data since both data are processed by the same algorithm except for the difference in radar sensitivity.

ACKNOWLEDGMENT

The authors would like to thank Hanado of the National Institute of Information and Communications Technology (NICT), Dr. R. Oki and Furukawa of the JAXA, Higashiuwatoko, Yoshida, and Masaki of the Remote Sensing Technology Center of Japan (RESTEC) for providing invaluable information and comments.

REFERENCES

[1] J. Simpson, R. F. Adler, and G. R. North, "A proposed tropical rainfall measuring mission (TRMM) satellite," *Bull. Amer. Meteorol. Soc.*, vol. 69, no. 3, pp. 278–295, 1988.

[2] C. Kummerow, W. Barnes, T. Kozu, J. Shiue, and J. Simpson, "The tropical rainfall measuring mission (TRMM) sensor package," *J. Atmos. Ocean. Technol*, vol. 15, pp. 809–817, Jun. 1998.

[3] N. Takahashi and T. Iguchi, "Estimation and correction of beam mismatch of the precipitation radar after an orbit boost of the tropical rainfall measuring mission satellite," *IEEE Trans. Geosci. Remote Sens.*, vol. 42, no. 11, pp. 2362–2369, Nov. 2004.

[4] S. Shimizu, R. Oki, T. Tagawa, T. Iguchi, and M. Hirose, "Evaluation of the effects of the orbit boost of the TRMM satellite on PR rain estimates," *J. Meteor. Soc. Jpn.*, vol. 87A, pp. 83–92, Mar. 2009.

[5] T. Tagawa, H. Hanado, S. Shimizu, and R. Oki, "Improved correction of beam mismatch of the precipitation radar after orbit boost of the TRMM satellite," *IEEE Trans. Geosci. Remote Sens.*, vol. 47, no. 10, pp. 3469–3479, Oct. 2009.

[6] A. Y. Hou *et al.*, "The global precipitation measurement mission," *Bull. Amer. Meteorol. Soc.*, vol. 95, pp. 701–722, May 2014.

[7] G. Skofronick-Jackson *et al.*, "The global precipitation measurement (GPM) mission for science and society," *Bull. Amer. Meteorol. Soc.*, vol. 98, pp. 1679–1695, Aug. 2017.

[8] T. Kozu *et al.*, "Development of precipitation radar onboard the tropical rainfall measuring mission (TRMM) satellite," *IEEE Trans. Geosci. Remote Sens.*, vol. 39, no. 1, pp. 102–116, Jan. 2001.

[9] T. Kozu, T. Iguchi, T. Shimomai, and N. Kashiwagi, "Raindrop size distribution modeling from a statistical rain parameter relation and its application to the TRMM precipitation radar rain retrieval algorithm," *J. Atmos. Ocean. Technol.*, vol. 48, no. 4, pp. 716–724, 2009.

[10] R. Meneghini *et al.*, "Use of the surface reference technique for path attenuation estimates from the TRMM precipitation radar," *J. Appl. Meteorol.*, vol. 39, no. 12, pp. 2053–2070, Dec. 2000.

[11] T. Tagawa, H. Hanado, K. Okamoto, and T. Kozu, "Suppression of surface clutter interference with precipitation measurements by spaceborne precipitation radar," *IEEE Trans. Geosci. Remote Sens.*, vol. 45, no. 5, pp. 1324–1331, May 2007.

[12] J. Awaka, T. Iguchi, and K. Okamoto, "TRMM PR standard algorithm 2A23 and its performance on bright band detection," *J. Meteor. Soc. Jpn.*, vol. 87A, pp. 31–52, Mar. 2009.

[13] T. Iguchi, T. Kozu, J. Kwiatkowski, R. Meneghini, J. Awaka, and K. Okamoto, "Uncertainties in the rain profiling algorithm for the TRMM precipitation radar," *J. Meteorol. Soc. Jpn.*, vol. 87A, pp. 1–30, Mar. 2009.